Available online at www.sciencedirect.com
SCIENCE DIRECT®
Pergamon
Cement and Concrete Research 34 (2004) 991–1000
CEMENT AND CONCRETE RESEARCH

Corrosion by chlorides in reinforced concrete: Determination of chloride concentration threshold by impedance spectroscopy

Olivier Poupard*, Abdelkarim Aït-Mokhtar, Paul Dumargue

LEPTAB, University of La Rochelle, 17042 La Rochelle, France

Received 5 February 2003; accepted 17 November 2003

Abstract

Chloride penetration in reinforced concrete induces depassivation of the steel rebars and initiation of the corrosion process leading to degradation of the structure. The coupling of ''low-frequency'' impedance response with SEM observations and multielementary analyses emphasized that the strong decrease of the capacitive part is related to the corrosion initiation. This experimentally determined incubation period is used in an electrodiffusion model based on Fick's second law to quantify the chloride concentration threshold responsible for corrosion initiation on the reinforcing steel surface. This work thus allowed quantifying the incubation period and the critical chloride concentration, referred to in Tuutti's diagram [K. Tuutti, Corrosion of steel in concrete, CBI Research Report no. 4.82, Swedish Cement and Concrete Research Institute, Stockholm, Sweden, 1982].

Keywords: Acceleration; Spectroscopy; Corrosion; Durability; Chloride; Cement paste

1. Introduction

Corrosion of reinforcing steel is of great concern because it is probably the most widespread cause of degradation in reinforced concrete. Initially, reinforcing steel embedded in concrete is naturally protected from corrosion by the high alkalinity of its interstitial solution [1]. However, this passive state can be inhibited by the destruction of the passive film by aggressive ions (chlorides, sulfates) or by an acidification of the environment near the rebar (carbonation). Corrosion of reinforcing steel is the natural result of chloride penetration in reinforced concrete. Tuutti [2] suggests that from the point of view of the reinforcement corrosion, the service life of a concrete structure can be subdivided into an incubation period (t_1) and a propagation period (t_2) (Fig. 1).

- The incubation period (t_1) corresponds to the chloride penetration within the porous materials and their accumulation in the vicinity of the rebar. Its duration depends on the concrete cover and on the chloride concentration required to start the corrosion process.
- The propagation period (t_2) corresponds to the stage when the chloride ions depassivate the reinforcing steel surface, leading to the development of the corrosion and, at term, to the local ruin of the structure.

Among the various electrochemical methods widely developed in the literature, electrochemical impedance spectroscopy (EIS) seems to be the most reliable technique in monitoring the corrosion process in reinforced concrete [3–6]. This method, contrary to the stationary techniques (anodic polarization method), allows the characterization, in a nondestructive way, of both the diffusion of aggressive species within the cement-based materials and the kinetics of electrochemical reactions that occur on the steel electrode surface.

The aim of this work is to study the chloride action on depassivation of a steel rebar embedded in a cement-based material and to quantify the incubation period t_1 (Fig. 1) through the use of the impedance method. Moreover, we will show how to determine the chloride concentration threshold required on the reinforcing steel surface to activate the corrosion process. For this purpose, an original accelerated monitoring procedure of the corrosion process of a reinforcing steel/cement-based material system is suggested. It is based on the combination of a nondestructive electrochemical method (EIS) and the application of a constant electric field.

* Corresponding author. Tel.: +33-5-46-45-72-48; fax: +33-5-46-45-82-41.
E-mail address: opoupard@univ-lr.fr (O. Poupard).

0008-8846/$ – see front matter © 2004 Elsevier Ltd. All rights reserved.
doi:10.1016/j.cemconres.2003.11.009

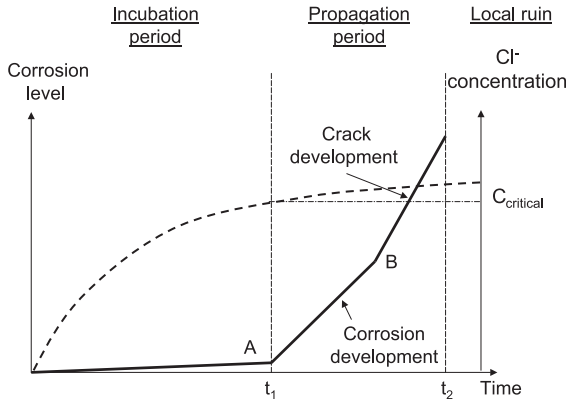

Fig. 1. Schematic sketch of steel corrosion sequence in concrete [2].

This electrical field is used to accelerate chloride ion transfer within the cement-based material.

2. Scope of the study

Impedance is commonly depicted as a complex function, having both real and imaginary components. It is usually plotted in the Nyquist diagram, as imaginary part vs. real part, providing a convenient tool for determining various electrical response behaviors. Fig. 2 presents a typical diagram for an electrochemical cell. The salient features of the spectrum are labeled as follows:

- the electrolyte resistance R_e given by the high-frequency limit of the diagram,
- the charge transfer resistance R_{CT} given by the diameter of the high-frequency loop,
- the polarization resistance R_P given by the low-frequency limit.

Although this typical behavior has not been systematically checked experimentally, researchers [6,7] have agreed to describe the impedance spectra in three distinct features over a large frequency domain (1 mHz–10 MHz): high, intermediate and low frequencies.

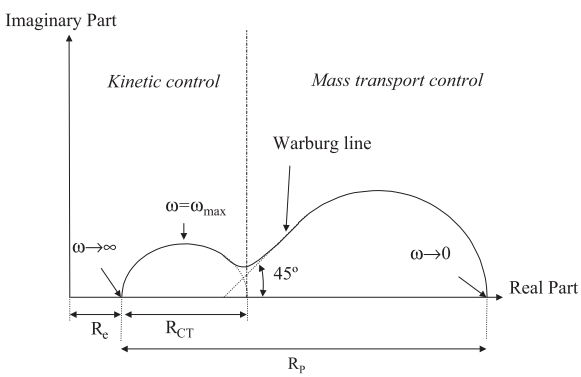

Fig. 2. Typical Nyquist diagram.

The low-frequency loop (1 mHz–10 Hz), referred to as the R_P parameter, varies according to the electrochemical state of the reinforcing steel surface.

Consequently, in the present work, we focus on the use of the impedance response in this low-frequency domain and on the evaluation of the R_P parameter variation.

3. Tests and materials

3.1. Cell and experimental setup

Fig. 3 presents the experimental cell based on the adaptation of an existing chloride electrodiffusion cell. A three-point configuration was used: a counter electrode (large platinum mesh), a working electrode (reinforcing steel) and a reference electrode [saturated calomel electrode (SCE)]. This configuration allows one to characterize the reaction phenomena, which take place only on the working electrode surface (reinforcing steel) [7]. The measurement setup consists of a potentiostat connected to a frequency response analyzer (FRA) (Fig. 3). The potentiostat applies a constant electric field (DC field) that accelerates chloride diffusion within the cement-based material. In parallel to this DC field,

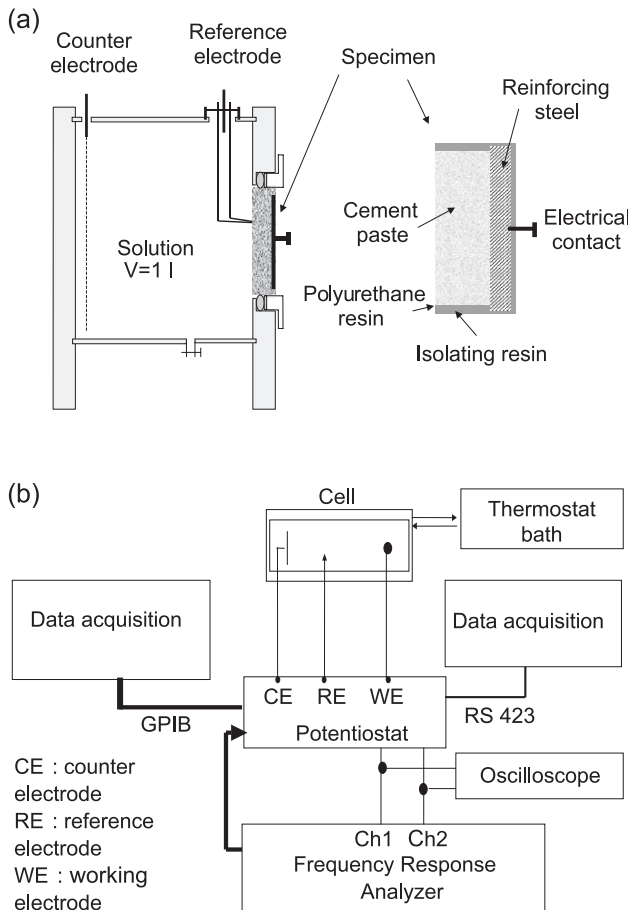

Fig. 3. (a) Experimental cell. (b) Schematic view of the experimental setup.

the FRA applies an alternating signal (AC field) to determine the impedance of the studied system. The amplitude of the signal is limited to 20 mV to ensure the linearity of the response (this value has been checked experimentally) [7]. The impedance data are recorded logarithmically down in the frequency range, from 5 mHz to 1 MHz.

3.2. SEM and multielementary analysis

The reinforcing steel surface was observed by using a Jeol 5410 LV scanning electron microscope after the corrosion test. In association with SEM observation, energy dispersive X-ray (EDX) analysis and multielementary cartography were performed to characterize the corrosion products.

3.3. Diffusion coefficient calculation

The diffusion coefficient measurement was performed from a classical electrodiffusion cell (Fig. 4). A potentiostat was used to apply a constant electric field across the cement-based material specimen. A four-point configuration was used (two platinum mesh and two reference electrodes) to control the potential imposed on the specimen's faces. The downstream compartment contains a simulated pore solution (0.025 M NaOH and 0.083 M KOH). The upstream compartment is filled with a similar solution with a known chloride concentration (0.5 M NaCl). The experimental procedure has been described by Amiri et al. [8]. Potentiometric titration tests with silver nitrate were performed in the downstream compartment after the NaCl addition. The measurement of the ionic flux in steady state allows one to deduce the diffusion coefficient D_{ss} from Eq. (1) [8]:

$$D_{ss} = \frac{RT}{z_{Cl^-}F}\frac{L}{U}\frac{\Delta C V_a}{\Delta t A C_0}\left(1 - e^{-\frac{zF}{RT}U}\right) \quad (1)$$

where V_a is the downstream compartment volume (m^3), A is the cross-section area (m^2), ΔC is the variation of chloride concentration in the downstream compartment during a time range Δt (mol/m^3), L is the specimen's thickness (m), C_0 is the chloride concentration in the upstream cell (500 mol/m^3), R is the gas constant (J/mol K), T is the reference temperature (K), z_{Cl^-} is the chloride ion valence, F is the Faraday constant (J/V mol) and U is the difference of potential (V).

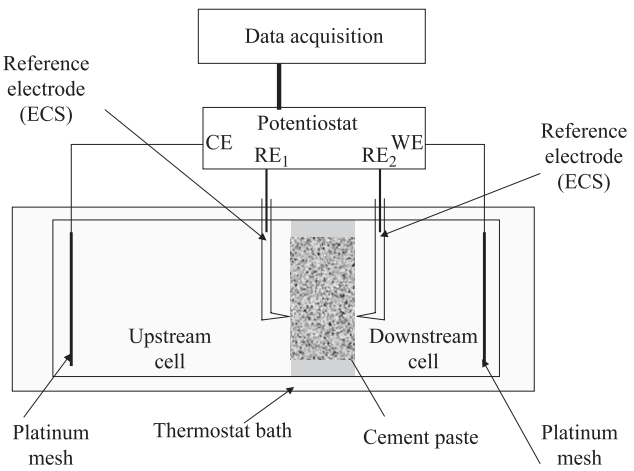

Fig. 4. Electrodiffusion cell.

Table 1
Composition and average thickness of specimens

Materials	Designation	w/c	Average thickness (mm)	Standard value (mm)
P0.7	P0.7(1)	0.7	1.1	0.02
	P0.7(2)	0.7	0.85	0.1
	P0.7(3)	0.7	1.04	0.01
P0.5	P0.5(1)	0.5	1.12	0.02
	P0.5(2)	0.5	1.09	0.02
	P0.5(3)	0.5	0.975	0.05
P0.3	P0.3(1)	0.3	1.12	0.02
	P0.3(2)	0.3	1.06	0.02
	P0.3(3)	0.3	0.975	0.02

3.4. Materials

The specimens were made up of a 65-mm-diameter reinforcing steel disc (type: Fe E24). After being sand-blasted and rinsed with deionized water, the disc is covered on one face with a cement-based material whose composition, manufacturing and conservation details are described below. The other face (electrically connected) and the side faces of the cement-based material/reinforcing steel system were covered with a polyurethane resin to limit the chloride transfer to a one-dimensional direction (Fig. 3).

For the impedance measurements, previous studies [9,10] have described the experimental protocol. It was shown that the transfer acceleration by the DC field had to be limited to 5 V/m (maximal value) in order to cancel some artifact measurements. This value allows a real but insufficient acceleration of the chloride transfer. Note that some natural exposure tests were performed (without applied electric field). However, after about 3 months, no impedance variation was observed. There were no signs of corrosion initiating at the steel surface. Therefore, we cannot actually check how much gain in test duration the external field provides. Some tests are yet in progress.

Consequently, to reduce the chloride transfer duration and to avoid long laboratory tests, we needed to limit the coating thickness to a few millimeters, which implies that the representativeness and the homogeneity of the material limit this study to the cement pastes.

After the core sampling of the cement paste on the reinforcing steel disc, a thickness of 1 mm is obtained by sawing and polishing the cement coating just before the accelerated tests.

For all specimens and tests (impedance measurements and electrodiffusion), the specimens manufactured have a prismatic form ($100 \times 100 \times 200$ mm^3). After demoulding (24 h after manufacturing), the specimens were cured for 28

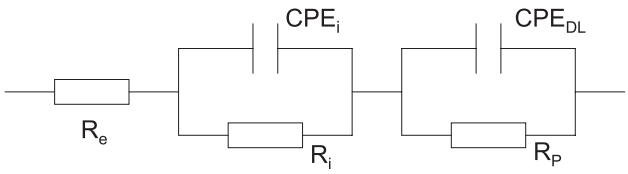

Fig. 5. Equivalent circuit model for impedance simulation.

days in an alkaline solution that is identical to that of the tests and simulates the cement-based material pore solution (0.083 M KOH and 0.025 M NaOH). This curing was performed to ensure the specimens' saturation and to reduce leaching.

To avoid wall effects, samples were obtained by a technique of core sampling to have a cylindrical form of 65-mm diameter and 10-mm thickness. The lateral surface was covered with epoxy resin to ensure a unidirectional chloride transfer (Fig. 3).

Cement pastes were made from Portland cement CEM-I 52.5 (according to European Standards EN 197-1) and deionized water. Three deionized water/cement (w/c) ratios were studied: 0.7, 0.5 and 0.3 referred to as P0.7, P0.5 and P0.3, respectively (see Table 1).

During the test, the specimens were exposed to the same solution with 0.5 M of NaCl added.

4. Results

4.1. Impedance measurements

The impedance spectra were modeled by using an equivalent circuit model (Fig. 5) in which the RC parameters were used to assist data interpretation. "Zplot" software was used for running experiments and fitting curves with the electrical circuit. Globally, the fit errors are less than 5%, except for P0.3 for which the fit errors on the calculation of R_P reached 20%.

Fig. 6 shows the impedance response at various time measurements, plotted in the Nyquist diagram for specimens P0.7, P0.5 and P0.3. The impedance response variations are similar for the three tested materials. Three phases are denoted:

- an increase of the capacitive part during the first hours,
- a stable phase (no significant variation of the impedance response) during a duration that would depend on the cement-based material mix,
- and a decrease of the capacitive part.

Fig. 7 presents the polarization resistance R_P evolution (obtained from the low-frequency impedance response) vs. time for P0.7, P0.5 and P0.3, respectively. Here again, the three tested materials show a similar trend: an initial increase, followed by a constant response and, finally, a decrease phase.

The reinforcing steel polarization induced by the applied electric field and the high alkalinity at the surface of steel make this possible later in a passive region during the first hours of the test. This supports passive film reinforcement and provides further protection of the steel against corrosion [11].

Thus, this adherent surface film slows down the corrosion rate of the reinforcing steel. This is described by the evolution over time of the polarization resistance R_P. The increase of R_P characterizes the reinforcement of this passive layer in an initial period. After a given time, the system stabilizes thermodynamically and R_P reaches a plateau (establishing

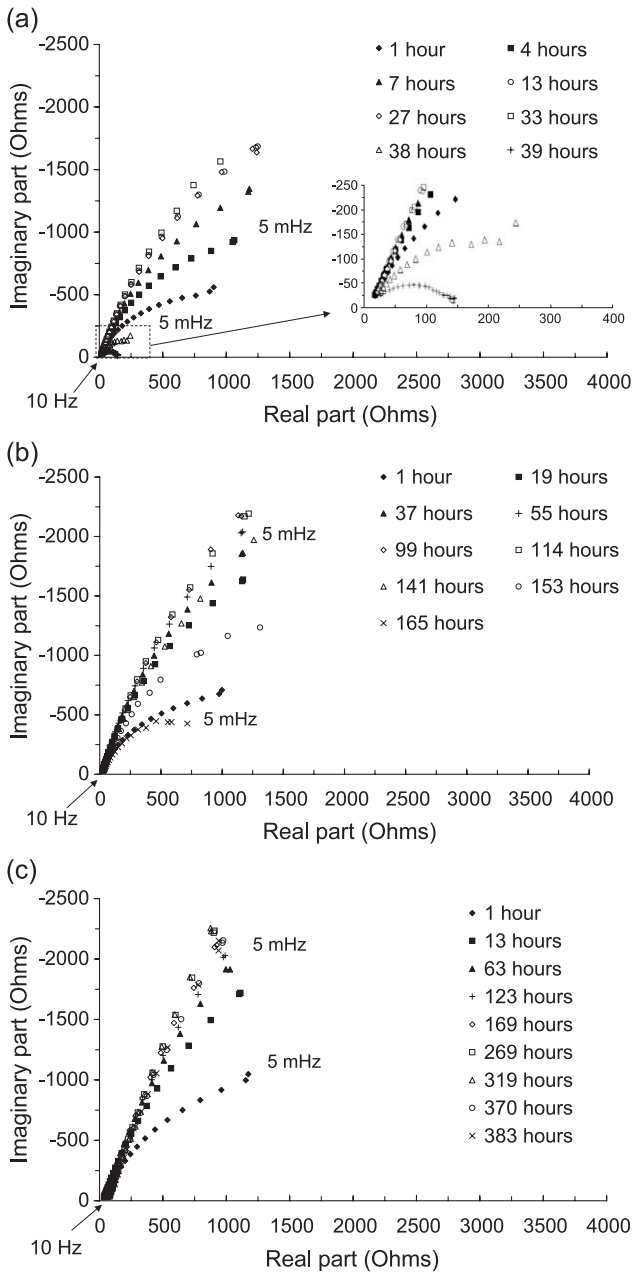

Fig. 6. Nyquist plots in low-frequency domain. (a) P0.7(1), (b) P0.5(1), (c) P0.3(1). Legend indicates exposure time.

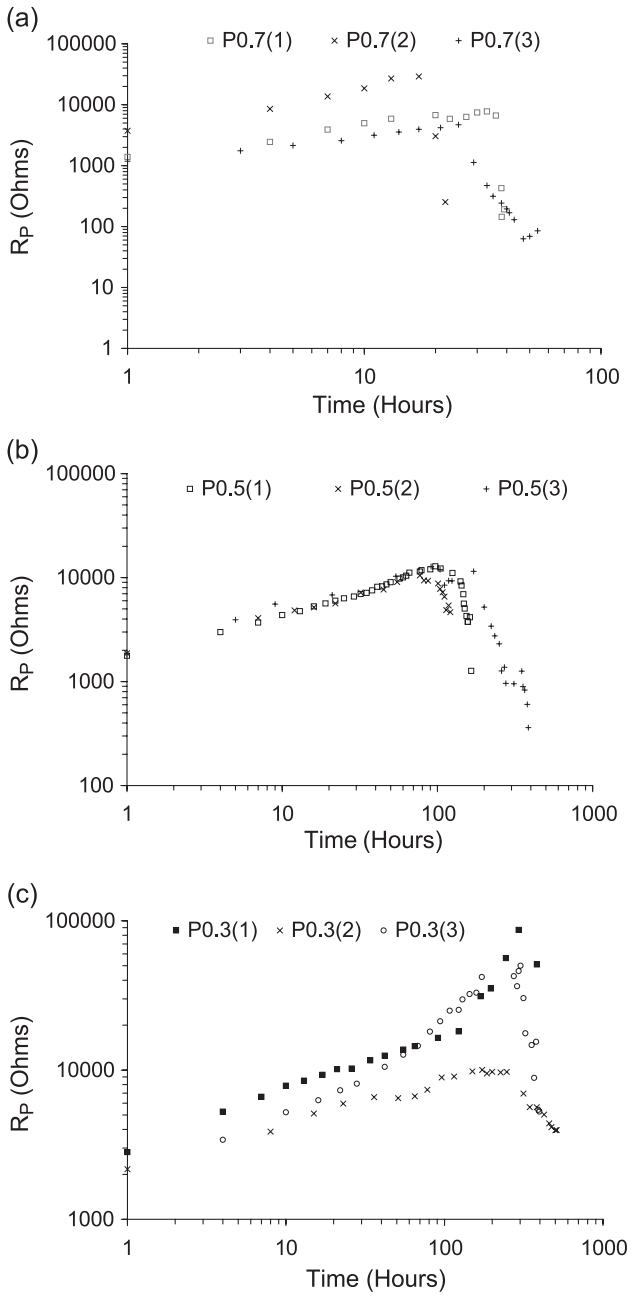

Fig. 7. Polarization resistance values vs. exposure time. (a) P0.7, (b) P0.5, (c) P0.3.

the combined protection: alkalinity and polarization). At the same time (increase and plateau), chlorides migrate within the cement-based material. When they reach the reinforcing steel surface in a sufficient quantity (which corresponds to the threshold value), they break the passive film and corrosion by pitting starts. This modifies the electrochemical processes at the reinforcing steel surface (anodic oxidation of steel with oxygen reduction) and causes the drop of the R_P value [10]. Again, it seems that the applied electrical field leads to an acceleration of the corrosion development, allowing better observation of the corrosion initiation.

Differences of R_P data for the same w/c ratio can be attributed to the microheterogeneity of the contact cement paste/steel and that of the steel surface (i.e., to the sand-blasting process), then to the heterogeneity of the passive film.

Further analysis was performed on other P0.5 specimens. Similar impedance procedure was followed. However, just at the beginning of the R_P value decrease, the cement coating was destroyed and the steel electrode surface was inspected by SEM (Fig. 8(a)) and EDX analysis (Fig. 8(b)) to control its passive state. Direct visual observation indicates that the corrosion process was activated. The reinforcing steel surface is not homogeneous because the whole surface has not undergone the same mechanisms. Two distinct areas were observed: one presenting a pitting corrosion and another one without corrosion products. The latter appeared to be rich in

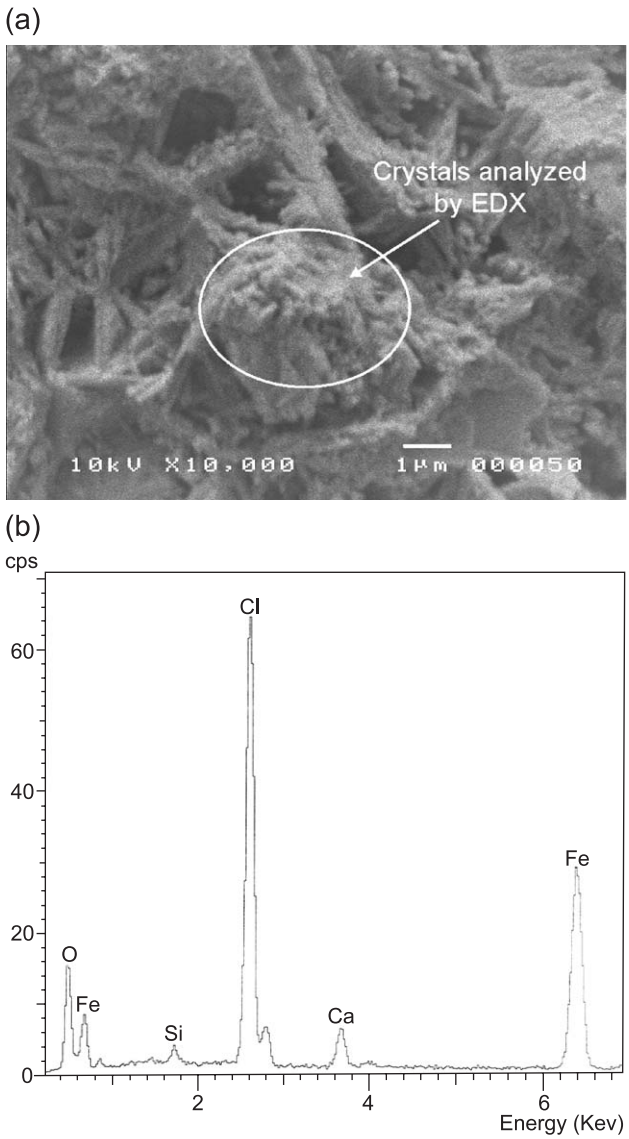

Fig. 8. (a) SEM micrograph showing the reinforcing steel surface after the decrease of the LF loop specimen P0.5(1); exposure time: 165 h. (b) EDX analysis of the crystals observed.

calcium and corresponds to the passive layer that protects the steel surface from aggressive environments.

4.2. SEM observations and EDX analysis

The corroded areas were observed by SEM (Fig. 8(a)). EDX analysis (Fig. 8(b)) details the composition of corrosion products on the electrode surface related to the chloride attack: except for iron, chloride and oxygen were detected.

An additional analysis was performed by the elaboration of a multielementary (Cl, Ca, Fe, O elements) cartography used to visualize the spatial distribution of these elements from the cross section of a specimen. Fig. 9(a) depicts the interface area between the reinforcing steel (white) and the cement paste (black) observed by SEM. The cartography (Fig. 9(b)) again confirms the presence of chloride (Picture 3) among the other elements at the steel/cement paste interface.

To conclude, these various analyses show that the beginning of the R_P value drop is associated with corrosion activation. Indeed, this localized corrosion process is associated with the breakdown of the protective passive film induced by the arrival of the chloride ions on the reinforcing steel surface. These results are in agreement with previous studies that have suggested a correlation between this resistance R_P and the corrosion rate (Stern–Geary equation) [12–14].

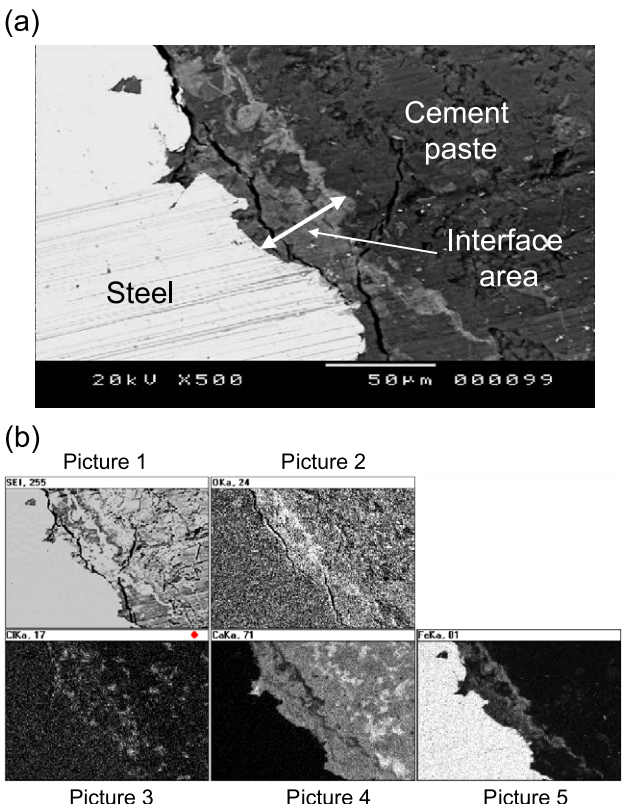

Fig. 9. (a) SEM micrograph of a cross section of a specimen after a corrosion test. (b) Multielementary cartography associated—O (Picture 2), Cl (Picture 3), Ca (Picture 4), Fe (Picture 5).

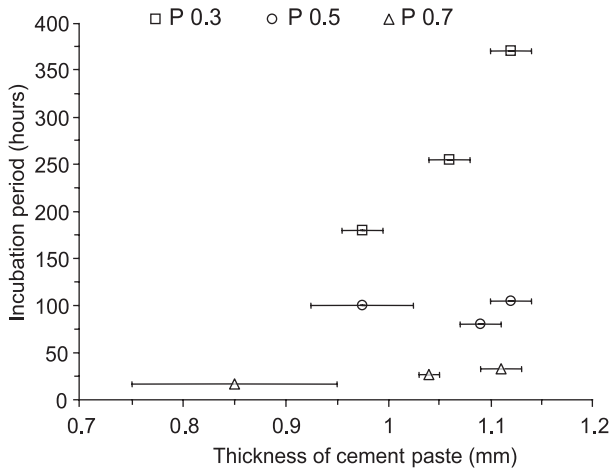

Fig. 10. Incubation period for the three studied materials.

4.3. Determination of the incubation period

The incubation period is deduced from the variation over time of the R_P polarization resistance, which is the time from which the diameter of the low-frequency loop begins to decrease. Fig. 10 shows the incubation period of the three studied materials for different average thicknesses of cement coatings. On this graph, the uncertainties associated with the inaccuracy of the thickness measurements are also noticed (see Table 1). The differences observed in Fig. 10 are due to the variation of the specimen thickness. As shown in Section 3.4, 1-mm thickness is an average value obtained from nine measurement points. Indeed, the polishing device does not allow obtaining a face exactly parallel to the reinforcing steel plan. Moreover, the variability in the porous structure, from one specimen to another (for a similar mix), also explains the nonhomogeneous evolution of the R_P resistance.

4.4. Critical threshold in chloride concentration

The incubation period is associated with a critical chloride concentration cumulated on the reinforcing steel

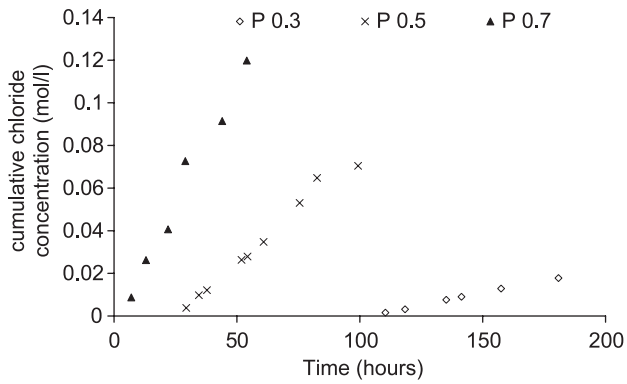

Fig. 11. Cumulative chloride concentration in the downstream compartment for the three studied materials.

Table 2
Diffusion coefficient values

Cement-based material	Porosity, ε_p	Diffusion coefficient of chloride ions, D_{ss} (m^2/s)
P0.3	0.1446	1.36×10^{-12}
P0.5	0.273	5.95×10^{-12}
P0.7	0.473	1.34×10^{-11}

surface. The determination of the concentration threshold responsible for the corrosion activation was the subject of some studies in the literature [15,16]. However, there is no agreement on an exact quantitative amount of chloride required for depassivating the reinforcing steel surface [17].

A first approach is proposed as an example of a methodology to quantify the critical chloride threshold level based on Fick's second law. It requires knowledge of the diffusion coefficient of the cement-based material.

4.4.1. Steady-state diffusion coefficient D_{ss}

Fig. 11 shows the cumulative chloride concentration in the downstream compartment vs. time for each studied w/c ratio (0.7, 0.5 and 0.3, respectively). The steady-state diffusion coefficient D_{ss} is deduced from Eq. (1) (Table 2). The diffusion coefficient increases with an increase of the w/c ratio. These results are in agreement with those of El-Belbol [18].

4.4.2. Adopted model

In a first approach, the time-dependent distribution of chloride concentration over the depth to which the steel is embedded can be obtained from the solution of Fick's modified second law assuming the cement-based material as a homogeneous semi-infinite medium.

This model has two main shortcomings. First, the material is heterogeneous (made of solid and liquid phases). Second, resolution conditions are not really adapted to our experimental configuration: because of the low thickness of the steel coating (1 mm), the boundary conditions are different from those corresponding to a semi-infinite electrodiffusion. Nevertheless, let us give a first approach.

According to Tang and Nilsson [19] and Xu and Chandra [20], for the initial condition $C(x,\ t=0)=0$ and boundary condition $C(x=0,\ t)=C_0$ (constant value), the chloride distribution at a depth x and a time t within a cement-based material under an electrodiffusion test is expressed by:

$$\frac{C(x,t)}{C_0} = \frac{1}{2} e^{\frac{z_{Cl^-} F E_e}{2RT} x} \left[e^{-\beta x} \operatorname{erfc}\left(\frac{x - 2\beta D_{nss} t}{2\sqrt{D_{nss} t}} \right) + e^{\beta x} \operatorname{erfc}\left(\frac{x + 2\beta D_{nss} t}{2\sqrt{D_{nss} t}} \right) \right] \quad (2)$$

where C_0 is the chloride concentration in the solution in contact with the cement-based material (mol/m^3), x is the depth (m) and E_e is the external electrical field (V/m).

$$\beta = \sqrt{\left(\frac{z_{Cl^-} F}{2RT} E_e \right)^2 + \frac{k}{D_{nss}}} \quad (3)$$

where D_{nss} is the non-steady-state diffusion coefficient. As referred to in Ref. [19], $D_{nss} = D_{ss}/[\varepsilon_p(1 + \partial c_b/\partial c)]$, where ε_p is the porosity of the cement-based material and $\partial c_b/\partial c$ is called chloride-binding capacity.

k is the binding rate between chlorides and hydrated components of the cement-based material (mainly C_3A).

The porosity ε_p was obtained from the w/c ratio by using Powers and Brownyard's model [21] (Table 2).

To monitor the concentration over time at the steel surface, the depth x must be equal to the thickness of the cement-based material. The diffusion coefficients have been previously calculated (Table 2) (see Section 4.4.1). The numerical values for the other parameters are: $E_e = 5$ V/m, $R = 8.314$ J/mol K, $F = 96{,}500$ C, $T = 303$ K, $z_{Cl^-} = -1$ and $C_0 = 500$ mol/m^3.

Fig. 12 shows the influence of the binding rate value on the chloride concentration profile at the steel surface. We note that the increase of k value induces a slight decrease of the chloride concentration. Consequently, it should be noted

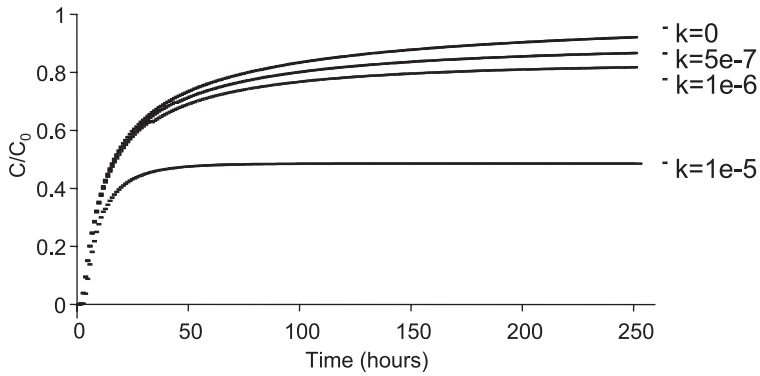

Fig. 12. Influence of the binding rate value, k, on profile of chloride concentration at the steel surface vs. exposure time for P0.5 sample.

that considering no binding rate between chlorides and hydrated components slightly overestimates the actual chloride concentration, as observed in Fig. 12.

Because of the lack of precise values in the literature and given its slight influence on the chloride concentration, the binding rate k was neglected.

4.4.3. Calculation of critical chloride concentrations

Fig. 13 shows, in similar graphs, the variations over time of the nondimensional chloride concentration at the reinforcing steel surface (given by Eq. (2)) and the R_P resistance, respectively (one example per w/c ratio). The critical threshold in chloride concentration corresponds to the beginning of the R_P resistance drop (obtained from impedance responses). Fig. 14 summarizes the results of the nondimensional chloride concentration required to activate the corrosion process for the tested materials.

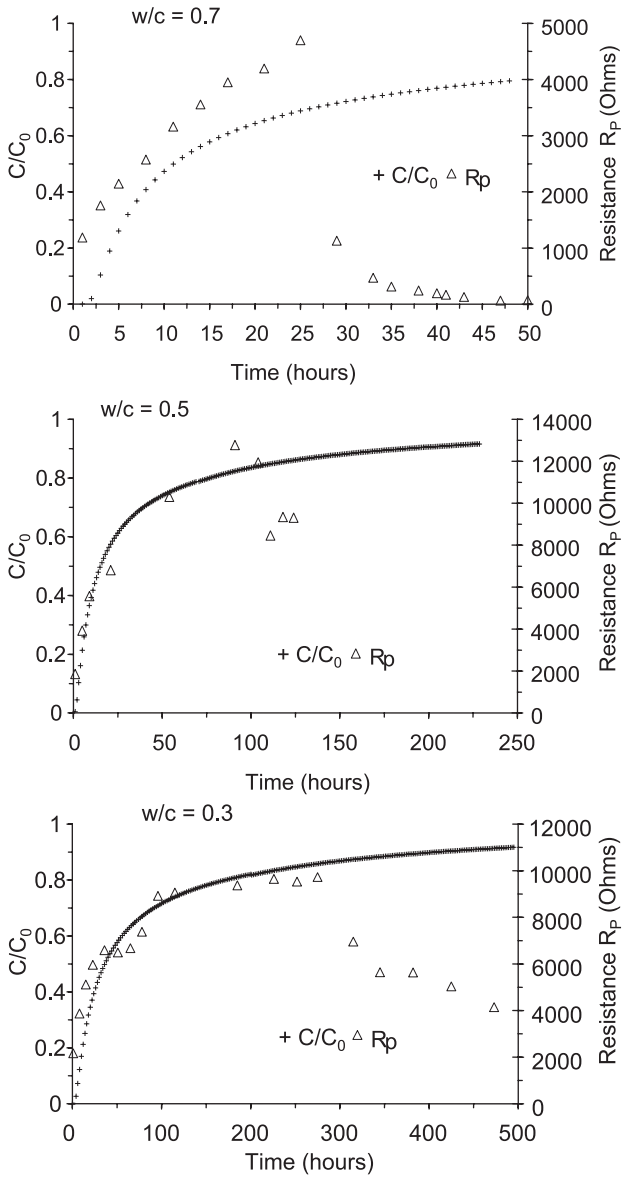

Fig. 13. Profile of chloride concentration at the steel surface and variation of R_P value (Δ) vs. exposure time for specimens P0.7, P0.5 and P0.3, respectively.

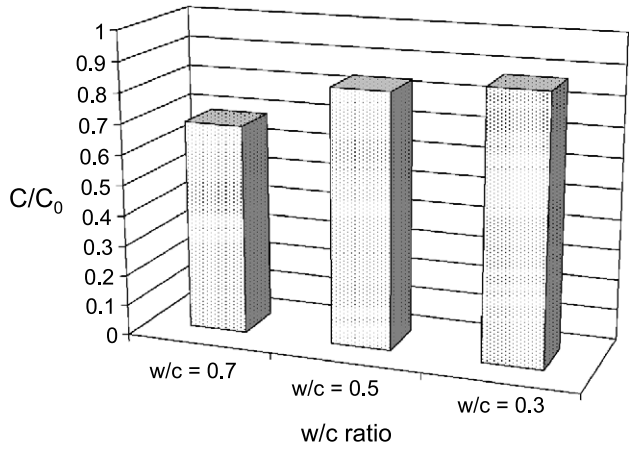

Fig. 14. Nondimensional chloride concentration corresponding to the critical threshold initiating the corrosion at the reinforcing steel surface.

5. Discussion

The results highlight the influence of the w/c ratio (i.e., porosity) on the chloride threshold level: we observe an increase of the chloride threshold level with the decrease of the w/c ratio. This emphasizes that the steel coating quality is an important factor that may affect the threshold level and, consequently, the service life of the structure.

This result is in agreement with those of some researchers [15,16]. Pettersson [15] reported that the threshold chloride concentration in pore solution expressed under pressure from mortar specimens with w/c ratios ranging between 0.75 and 0.3 varied between 0.28 and 1.8 mol/l. This behavior is attributed to the decrease in the pH of the concrete pore solution by the dilution effect of an increasing of w/c ratio and to the modification of the chloride-binding capacity. It is well known that voids at the steel–concrete interface have a significant effect on the chloride threshold level attributed to the absence of calcium hydroxide at these locations that would otherwise resist a local fall in pH [17].

Thus, the differences observed between the experimental results seem to be mainly due to the disparities between the thickness values that constitute the average thickness of the specimens (see Table 2).

The R_P variations over time (Fig. 7) highlight the high sensitivity of the impedance response to the microstructure properties of the cement-based material: any variation of these properties has a great influence on the required time to initiate the R_P drop, and, consequently, to activate the corrosion process. The differences between the thicknesses also explain the localized nature of the corrosion, which occurs at the reinforcing steel surface (pitting corrosion). However, Fick's second law does not take into account these

heterogeneities. It assumes a homogeneous front of chlorides. This point has to be improved.

Lastly, as shown by the multielementary analyses (Figs. 8 and 9), chlorides are not the only species responsible for the activation of the corrosion process. The oxygen (as hydroxyl ions, OH^-) also acts [22,23].

6. Conclusion

A first approach of a useful tool to determine in a comparative way the concentration threshold value to initiate the corrosion of a reinforcing steel embedded in a cement-based material is proposed.

The results highlight the correlation between the impedance response and the corrosion activation. The coupling of the impedance spectra in the low-frequency domain with the SEM observations and the multielementary analyses showed that the strong decrease of the capacitive part in the impedance response is linked to the chloride corrosion initiation.

This relationship leads to the quantification of the incubation period required to activate the corrosion process previously qualitatively defined by Tuutti [2]. This period corresponds to a chloride concentration threshold responsible for the corrosion initiation on the reinforcing steel surface. This concentration threshold was quantified from Fick's modified second law.

However, the corrosion observed by SEM was localized (pitting corrosion). This form of corrosion, due to the heterogeneity of the cement-based material, highlights the limitations of Fick's second law to describe the chloride transfer within the cement-based materials. Moreover, the model used, based on a semi-infinite electrodiffusion, does not allow considering in a correct way the boundary conditions of our experimental configuration. Therefore, it would be useful to improve the modeling by carrying out an appropriate model in which the chemical bindings between chlorides and hydrated components will be taken into account to reduce the calculated chloride threshold concentration uncertainties. In addition, the multielementary analyses have shown that chlorides are not the only species that play a role in the corrosion activation. Other ionic species, as hydroxyl ions, also participate. Therefore, it is necessary to complete this study by taking into account the action of these elements in the corrosion development in reinforced concrete. That will allow proposing some quantitative relationships that may be used to refine the threshold level for a known set of conditions.

As is proposed in this work, this methodology may be used as a comparative test only, since the external field to which specimens were exposed during the tests leads to some distortions in the steel behavior. Similar tests, without external field, are in progress in order to improve this method by attempting to correlate the results obtained with the steel behavior under natural conditions, especially for the relationship between the evolution of R_P parameter and that of the corrosion process.

To conclude, we plan to extend our study using more realistic specimens (made up of concrete), the final objective being the prediction of the service life of structures.

References

[1] A. Neville, Chloride attack of reinforced concrete: an overview, ACI Mater. Struct. 28 (1995) 63–70.
[2] K. Tuutti, Corrosion of steel in concrete, CBI Research Report no. 4.82, Swedish Cement and Concrete Research Institute, Stockholm, Sweden, 1982.
[3] P. Lay, P.F. Lawrence, N.J.M. Wilkins, D.E. Williams, An AC impedance study of steel in concrete, J. Appl. Electrochem. 15 (1985) 755–766.
[4] L. Hachani, C. Fiaud, E. Triki, Characterization of steel/concrete interface by electrochemical impedance spectroscopy, Br. Corros. J. 29 (2) (1994) 122–127.
[5] P. Gu, S. Elliott, R. Hristova, J.J. Beaudoin, R. Brousseau, B. Baldock, A study of corrosion inhibitor performance in chloride contaminated concrete by electrochemical impedance spectroscopy, ACI Mater. J. 94 (5) (1997) 385–395.
[6] S.J. Ford, J.D. Shane, T.O. Mason, Assignment of features in impedance spectra of the cement-paste/steel system, Cem. Concr. Res. 28 (12) (1998) 1737–1751.
[7] R. MacDonald, Impedance Spectroscopy: Emphasizing Solid Materials and Systems, Wiley, New York, 1987.
[8] O. Amiri, A. Aït-Mokhtar, P. Dumargue, Optimisation de l'essai d'électro-diffusion d'ions chlorures dans le béton, Rev. Fr. Gén. Civ. 4 (2–3) (2000) 161–173.
[9] O. Poupard, A. Aït-Mokhtar, P. Dumargue, Impedance spectroscopy in reinforced concrete: procedure for monitoring steel corrosion: Part I. Development of the experimental device, J. Mater. Sci. 38.
[10] O. Poupard, A. Aït-Mokhtar, P. Dumargue, Impedance spectroscopy in reinforced concrete: Procedure for monitoring steel corrosion: Part II. Polarization effect, J. Mater. Sci. 38 (2003) 3521–3526.
[11] M. Pourbaix, Thermodynamics and corrosion, Corros. Sci. 30 (10) (1990) 963–988.
[12] M. Stern, A. Geary, A theoretical analysis of the shape of polarization curves, J. Electrochem. Soc. 104 (1) (1957) 56–63.
[13] D.G. John, P.C. Searson, J.L. Dawson, Use of AC impedance technique in studies on steel in concrete in immersed conditions, Br. Corros. J. 16 (2) (1981) 102–106.
[14] C. Andrade, V. Castelo, C. Alonso, J.A. Gonzalez, The determination of the corrosion rate of steel embedded in concrete by the polarization resistance and AC impedance methods. In: V. Chaker (Ed.), Corrosion effect of stray currents and the technique for evaluating corrosion of rebars in concrete, ASTM STP 906, American Society for Testing and Materials, Philadelphia, 1986, pp. 43–63.
[15] K. Pettersson, Chloride threshold value and the corrosion rate in reinforced concrete, Cem. Concr. Res. 20 (1994) 461–470.
[16] G.K. Glass, N.M. Hassanein, N.R. Buenfeld, Neural network modelling of chloride binding, Mag. Concr. Res. 49 (1997) 323–335.
[17] G.K. Glass, N.R. Buenfeld, The presentation of the chloride threshold level for corrosion of steel in concrete, Corros. Sci. 39 (1997) 1001–1013.
[18] S.M.T. El-Belbol, Acceleration of chloride ion diffusion in concrete, Thesis, London University, England, 1990.
[19] L. Tang, L.O. Nilsson, Accelerated methods for chloride diffusivity and their application in prediction for chloride penetration, in: K. Scrivener, J.F. Young, (Eds.), Mechanisms of Chemical Degradation of Cement-Based Systems, E&F N Spon, 1996.

[20] A. Xu, S. Chandra, A discussion of the paper "Calculation of chloride diffusion coefficients in concrete from ionic migration measurements" by C. Andrade, Cem. Concr. Res. 24 (2) (1994) 375–379.
[21] T.C. Powers, T.L. Brownyard, Studies of the physical properties of hardened Portland cement pastes, J. Am. Concr. Inst. 43 (1947) 101, 249, 469, 549, 669, 845, 993.
[22] J.J. Carpio Perez, Etude de la dépassivation et de la repassivation des armatures métalliques dans les bétons, PhD thesis, LCPC, 1991.
[23] J.A. Gonzalez, S. Feliu, P. Rodriguez, E. Ramirez, C. Alonso, C. Andrade, Some questions on the corrosion of steel in concrete Part I: When, how and how much steel corrodes, Mater. Struct. 29 (1996) 40–46.